

## Optimal integration of DER and SST in active distribution networks

Funjun Meng<sup>a</sup>, Badrul Chowdhury<sup>b,\*</sup>, Md Shakawat Hossan<sup>b</sup>

<sup>a</sup> Electric Power Research Institute, China

<sup>b</sup> University of North Carolina at Charlotte, United States



### ARTICLE INFO

#### Keywords:

Distributed energy resources  
Distribution system operator  
Energy management  
Primal-dual interior point method  
Solid state transformer  
Optimal power flow

### ABSTRACT

The power distribution system is evolving towards a smart grid paradigm facilitated by infrastructure improvement, innovative technologies, and electronically-interfaced devices. The solid state transformer (SST) promises to be one of the most significant power electronically-interfaced devices to be integrated in the next generation distribution network due to its extensive energy management capability to handle interconnected AC and DC source(s) and load(s). In this paper, a three-phase unbalanced Optimal Power Flow (OPF) algorithm is extended for integrating distributed energy resources (DER) and SSTs in the future distribution networks. The purpose of the OPF is to optimize the economic operations of DERs in conjunction with the SST to improve system efficiency and voltage profiles, while controlling DER penetration. The topology and functionalities of the SST are introduced and modeled in the OPF algorithm. Comprehensive models of loads, conductors, voltage regulators, transformers, and pricing schemes are considered for accuracy. Based on the theoretical foundations, simulations are conducted on the IEEE 123 bus test system. The entire algorithm is also visualized in a quasi-static time-series (QSTS) manner to capture the variability of the system and response of the SSTs in different control modes. This can be adopted by distribution automation enterprises for active distribution networks.

### 1. Introduction

The electric power industry is undergoing profound changes as it moves toward a smart grid (SG) paradigm to achieve higher levels of energy efficiency, renewable energy resource integration, economic benefits, system reliability, and security [1]. Most restructuring, thus far, has taken place at the transmission or sub-transmission levels, while a majority of distribution systems continue to operate as monopolies with aging infrastructures. Traditional distribution system operators (DSOs) have limited options to purchase power from customers. In most cases, they procure power at wholesale prices from generation companies in the forward and/or futures market, and sometimes in the spot market, and supply their customers directly through distribution feeders at fixed electricity rates set by regulatory bodies [2]. However, distribution systems are evolving as a result of an infusion of smart grid technology and an increasing penetration of DERs. DERs are variable sized power generation units located at or close to customers. Various types of DERs are currently available which include conventional or micro-turbine generators (fueled by natural gas, diesel, etc.) and renewables (wind, solar photovoltaic or solar thermal, biomass, etc.). High penetration of DERs can create bi-directional power-flow complexity for many applications. However, in the envisioned smart

distribution system, high penetration of DERs can create a new window for DER owners to participate in economic operations as independent entities or market players [3]. Therefore, DSOs of today are beginning to feel the urgency to adopt a vastly different operational paradigm. In the new environment, DSOs can take more active role in command and control in the presence of increasing DER penetrations, leading to potentially better economic benefits and quality of energy service to customers [4]. A similar type of operation of DSOs has been observed in France to increase the reliability of distribution system [5].

The SST has drawn significant attention from the research community due to its extensive energy management capability with real and reactive power control. Besides, it has a reduced size and weight compared to the conventional iron-core type transformers with plug and play capability. Moreover, it can handle different types of AC and DC sources, and loads together [6,7]. For instance, the SST can deal with a combination of DERs, energy storage systems (ESS), and loads. Recent advancements in the power semiconductor technology have accelerated the utilization and commercialization of the SST with in-built parallel inverters, which has raised its potential to replace or supplement the conventional distributed transformers [8–11]. SSTs are also able to control voltage and power balance for higher energy efficiency [12,13]. Over the past few years, research efforts have targeted

\* Corresponding author.

E-mail address: [b.chowdhury@uncc.edu](mailto:b.chowdhury@uncc.edu) (B. Chowdhury).

<https://doi.org/10.1016/j.ijepes.2018.07.035>

Received 26 March 2018; Received in revised form 31 May 2018; Accepted 16 July 2018

Available online 27 July 2018

0142-0615/ © 2018 Elsevier Ltd. All rights reserved.

MVA level substations for SST installation [7,14,15].

As discussed earlier, since the SST can be considered as the future energy management device to integrate various types of DERs and loads in distribution systems, an OPF is needed for the operational scheme. The OPF needs to consider the conventional unbalanced distribution feeder with mixed phases (single, double, and three phase), non-linear loads, and other voltage regulating devices. These considerations can create more realistic scenarios for dispatching high DER penetration and economic operation by maintaining the security constraints such as, voltage and reactive power support. The OPF should also be generalized so that the modifications for SSTs can be included. Several OPF methodologies are suggested in the literature considering different objectives with different techniques for accurate and faster convergence. A second-order convex relaxation is proposed for fast-scale smart inverter response to control the reactive power and voltage profile in distribution systems with high PV penetration [16,17]. An optimal solution for real and reactive power inverter set point is proposed in [18] to bridge the temporal gap between long-term optimization and real-time inverter control. This method improves the system efficiency and stability with the participation of PV owners in the network. The authors utilized  $\epsilon$ -subgradient method with semidefinite programming relaxations to bypass the non-convexity of AC OPF formulation. A locational marginal price (LMP) based policy constraint is presented in [19] with high DER penetration to incentivize DER participation for reducing energy losses in distribution systems. They proposed a mathematical model using co-operative game theory by specifying the share of each DER unit in the reduced loss. An optimization routine is created in [20] for dispatching power from DERs and other sources using least-cost dispatch. A cost-causality-based tariff, which uses nodal pricing to recover the cost of losses, is employed in [21] over a tariff that averages the cost of losses and the Amp-mile method is used to recover the fixed network costs. The authors compared the tariff change with and without a DER integrated network from Uruguay. In [22], a genetic algorithm (GA) is used for optimal placement and sizing of DER to maximize the profit of DSOs. The authors evaluated the profit based on reduced losses in the presence of DER, and the electricity cost with and without incorporating DER. Voltage profile improvement is also considered in their methodology. Moreover, it is now widely accepted that system performance can be enhanced by integrating energy storage. Therefore, a second order cone programming (SOCP) OPF formulation is used in [23] to allocate dispersed storage systems (DSSs) while minimizing line current flows and load curtailment and maximizing DSS round-trip efficiency.

In this paper, a three-phase unbalanced OPF algorithm, presented in [24], is extended to solve the optimal integration of DERs and SSTs. It uses the primal-dual interior point method (PDIPM), which is widely recognized for its ability to solve non-linear optimization problems [25]. In [26], PDIPM is used to balance the phase voltages by injecting reactive power from the PV based DERs. The algorithm is also used in [27] to reduce the generation cost. The Hessian inverse matrix was used to check the convergence of the algorithm. In our work, we have used the Karush–Kuhn–Tucker (KKT) optimality conditions with three other criteria to check the convergence [25]. This paper uses additional variables for generation cost from DERs and substation using piecewise and quadratic representations, respectively. The algorithm features the rectangular coordinate format as used in current injection method (CIM) power flow analysis [28], and is adaptive to handle comprehensive and non-linear models of constant impedance, current, or power (ZIP) loads and different branch elements. It may be customized to adopt new devices or new constraints. The modifications to the OPF formulation for SST implementation is categorized and included in the algorithm. The SST has different control modes, two of which are – unity power factor (UPF) and var control modes. The latter enables the SST to operate as a controllable reactive power source that can be optimally operated by the DSOs using OPF analysis [12]. Both control methodologies are demonstrated in simulation results and compared

with traditional transformers. Compared to the OPF in the literature, the features of this OPF can be summarized below:

- A three-phase unbalanced OPF is extended for the integration of DER and SST. The objective of the OPF is to minimize the generation cost in the presence of SST.
- Marginal generation and shadow price are demonstrated for different control modes of SST and compared with the conventional case.
- Convergence of the OPF is tested using four different criteria to assure the optimal solution within the security limits.

The entire simulation is done in MATLAB on the IEEE 123 bus test system. To strengthen the analysis, a quasi-static time-series (QSTS) simulation is also conducted using the proposed OPF for voltage profile analysis.

## 2. Distribution feeder modeling

Precise modeling of distribution feeders leads to more accurate results for OPF problems. All the components of a typical feeder are described below.

### 2.1. Component modeling

A pi-model for branch elements in a distribution network is shown in Fig. 1. The general equations relating the nodal voltages at both ends of the branch ( $V_i$  and  $V_j$ ) and the branch currents at the two ends ( $I_i$  and  $I_j$ ) are given in (1) and (2).

$$\begin{bmatrix} I_i^{abc} \\ I_j^{abc} \end{bmatrix} = \begin{bmatrix} Y_{ii} & Y_{ij} \\ Y_{ji} & Y_{jj} \end{bmatrix} \begin{bmatrix} V_i^{abc} \\ V_j^{abc} \end{bmatrix} \quad (1)$$

where

$$Y_{ii} = C_{ii} \frac{Y_A}{a_T a_T^*} + Y_B, Y_{ij} = C_{ij} \frac{Y_A}{a_T^*}, Y_{ji} = C_{ji} \frac{Y_A}{a_T}, Y_{jj} = C_{jj} Y_A + Y_B. \quad (2)$$

$i, j \in \mathbb{Z}$  denotes the sending and receiving nodes, respectively where  $i \neq j$ .  $Y_A$  and  $Y_B$  represent the three-phase series and shunt admittance matrices of branch element, respectively;  $a_T$  refers to three-phase voltage ratio matrix; and  $C$  corresponds to the transforming matrices defined in Table 1. where

$$C_I = \begin{bmatrix} 1 & 0 & 0 \\ 0 & 1 & 0 \\ 0 & 0 & 1 \end{bmatrix}, C_{II} = \frac{1}{3} \begin{bmatrix} 2 & -1 & -1 \\ -1 & 2 & -1 \\ -1 & -1 & 2 \end{bmatrix}, C_{III} = \begin{bmatrix} -1 & 1 & 0 \\ 0 & 1 & 1 \\ 1 & 0 & 1 \end{bmatrix}.$$

The detailed models of each type of conductor is explained in the following parts.

#### 2.1.1. Conductor

The impedance matrix of the untransposed 3-wire or 4-wire conductors can be calculated using Carson's equations [29]. Since all conductor segments are connected in Y or Y-G with no off-nominal turns ratio change, the voltage ratio matrix  $a_T$  and all the transforming matrices,  $C$  are considered as diagonal identity matrix ( $C_I$ ).

#### 2.1.2. Transformer

Three phase transformers in distribution systems may have many

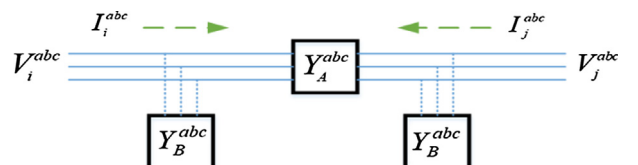


Fig. 1.  $\pi$ -model diagram for branch elements.

**Table 1**  
Transforming matrices of self and mutual admittance matrices for branch elements.

Branch Element	Connection Type	Self-Admittance		Mutual Admittance	
		$C_{ii}$	$C_{jj}$	$C_{ij}$	$C_{ji}$
Transformer or Voltage Regulator	Y-G → Y-G	$C_I$	$C_I$	$C_I$	$C_I$
	Delta → Delta	$C_{II}$	$C_I$	$C_{II}$	$C_{III}$
	Delta → Y-G	$C_{II}$	$C_{II}$	$C_{II}$	$C_{II}$

different connections (Y, Y-G, and Δ) on the primary and secondary sides. The voltage ratio matrix  $a_T$  is usually specified in the system configuration. The transforming matrices  $C_{xx}$  are listed in Table 1 for three most commonly used connection types.

### 2.1.3. Voltage regulator

Voltage regulators are important devices in conventional distribution systems for regulating or compensating voltage drops along the feeder. They can be treated as special autotransformers with a load tap changing mechanism. Standard step regulators contain a reversing switch enabling a ± 10% regulating range of voltages, usually in 32 steps. Assuming the tap change mechanism is installed at the primary side, the equivalent voltage ratio matrix  $a_T$  is basically determined by the tap positions and the type of regulator (type A or type B) [29].

$$a_T = 1 \pm .00625Tap^{abc} \tag{3}$$

where  $Tap^{abc} = 1, 2, \dots, 16$ . After obtaining all branch element admittance matrices, the system nodal admittance matrix  $Y_{BUS}$  can be built in rectangular coordinate as:

$$\begin{bmatrix} I_{M,1}^{abc} \\ I_{R,1}^{abc} \\ \vdots \\ I_{M,n}^{abc} \\ I_{R,n}^{abc} \end{bmatrix} = \underbrace{\begin{bmatrix} B_{11}^{abc} & G_{11}^{abc} & \dots & B_{1n}^{abc} & G_{1n}^{abc} \\ G_{11}^{abc} & -B_{11}^{abc} & \dots & G_{1n}^{abc} & -B_{1n}^{abc} \\ \dots & \dots & \ddots & \dots & \dots \\ B_{n1}^{abc} & G_{n1}^{abc} & \dots & B_{nn}^{abc} & G_{nn}^{abc} \\ G_{n1}^{abc} & -B_{n1}^{abc} & \dots & G_{nn}^{abc} & -B_{nn}^{abc} \end{bmatrix}}_{Y_{BUS}} \begin{bmatrix} V_{R,1}^{abc} \\ V_{M,1}^{abc} \\ \vdots \\ V_{R,n}^{abc} \\ V_{M,n}^{abc} \end{bmatrix} \tag{4}$$

where  $I_R, V_R, I_M,$  and  $V_M$  are the real and imaginary parts of complex current and voltage, respectively.  $G_{BUS}^{abc}$  and  $B_{BUS}^{abc}$  are the three-phase conductance and susceptance matrices in nodal matrix  $Y_{BUS}$ , respectively. By ordering the rows and columns,  $Y_{BUS}$  can be rewritten in decoupled format of real and imaginary parts as:

$$\begin{bmatrix} I_R^{abc} \\ I_M^{abc} \end{bmatrix} = \underbrace{\begin{bmatrix} Y_{RR} & Y_{RM} \\ Y_{MR} & Y_{MM} \end{bmatrix}}_{Y_{BUS}} \begin{bmatrix} V_R^{abc} \\ V_M^{abc} \end{bmatrix} \tag{5}$$

The branch admittance matrices  $Y^f$  and  $Y^t$  at “from” and “to” ends are found using the nodal admittance matrices  $C^f$  and the incidence matrices  $C^t$ . The incidence matrices indicate the connection relationship between nodes and branches.

$$\begin{bmatrix} I_R^{f,abc} \\ I_M^{f,abc} \end{bmatrix} = \begin{bmatrix} Y_{RR}^{f,abc} & Y_{MR}^{f,abc} \\ Y_{MR}^{f,abc} & Y_{MM}^{f,abc} \end{bmatrix} \begin{bmatrix} V_R^{f,abc} \\ V_M^{f,abc} \end{bmatrix} \tag{6}$$

where

$$Y_{RR}^f = C^f Y_{RR}, \quad Y_{RM}^f = C^f Y_{RM}, \tag{7}$$

$$Y_{MR}^f = C^f Y_{MR}, \quad Y_{MM}^f = C^f Y_{MM}. \tag{8}$$

The “to” end entries can also be found using the same formulation presented above by substituting “f” with “t”.

## 2.2. Nodal injection elements

### 2.2.1. ZIP load

Loads in distribution systems can be categorized by the method of connection to the primary feeder as distributed or spot load, in Y or Δ connection. In this study, distributed loads are converted to spot loads by lumping at the two ends of the line segment with proportion factors  $a$  and  $1-a$ , respectively. The active loads can be characterized as constant impedance ( $Z_p$ ), current ( $I_p$ ), or power ( $P_p$ ), known as ZIP loads. The equivalent power demand of ZIP loads  $P_{ZIP}$  is related to nodal voltage magnitudes which can be presented as [30]:

$$P_{ZIP} = P_o(Z_p \cdot |V|^2 + I_p \cdot |V| + P_p) \tag{9}$$

The above equation reflects the active power only. Similar formulation can be found for reactive power as well. Such nonlinear characteristic of ZIP loads is included in the OPF algorithm during the evaluation of the non-linear nodal balance constraints.

### 2.2.2. DER

DERs are controllable power injection units in the OPF algorithm. DER technologies whose primary outputs are direct current (e.g. solar photovoltaic and fuel cell technologies) mostly inject active power using a conventional inverter. This is also applicable for those DERs whose primary outputs are alternating current (e.g. wind and micro-turbine) by forcing them to operate at unity power factor to maximize the energy conversion efficiency. In economic operation analysis, the DER generation costs are given either as traditional quadratic function or as piecewise price segment. The piecewise cost functions are usually expressed using pairs of constant energy cost (\$/MWh) within specific range of generating power (MW or kW). These discontinuous segments can be converted into a continuous linear cost function  $f_{pw}$  as shown in [31,32] and will be discussed in the next section.

### 2.2.3. Solid state transformer

The SST is an advanced power electronic conversion device which contains three stages of single phase converters that are connected in cascaded mode: AC/DC active rectifier, dual active bridge (DAB) DC/DC converter, and DC/AC inverter, as shown in Fig. 2 in Section 3. There are two DC links in SST: low voltage DC (LVDC) and high voltage DC (HVDC), which act as a buffer between the primary feeder and the load. Voltages at HVDC and LVDC are regulated to constant values by the active rectifier and DAB converter, respectively. The SST node can be considered as a PQ node for power flow analysis. The net power flow at the primary side of the SST is the aggregated power injection/consumption from load and DER. In general, the SST provides several advanced features which are presented below:

- The reactive power injection at the rectifier primary side is regulated by the Q axis current  $I_q$  using a DQ vector controller [17]. The value of  $I_q$  depends on the external reactive power control signal ( $Q_{SST}^*$  in Fig.2. SSTs in var control mode are considered as controllable sources that can be optimally controlled by the DSOs using the OPF program. SSTs can also work at UPF mode without external var control signals.
- The LVDC serves as plug and play coupling hub, with constant regulated voltage, for DER or other types of distributed resources in either AC or DC types.
- The third stage inverter provides 1.0 p.u. AC voltage output to loads under normal conditions and also during voltage sag/swell events [6]. This exclusive functionality improves the power quality and reliability in energy services, significantly. Moreover, the constant terminal voltage will equivalently change the ZIP load into constant PQ load.
- The reactive power demand and injections from load and DER are filtered out at the DAB and the DC links if there is enough kVA rating at the converter, as shown in (10). Thus, the reactive power at the

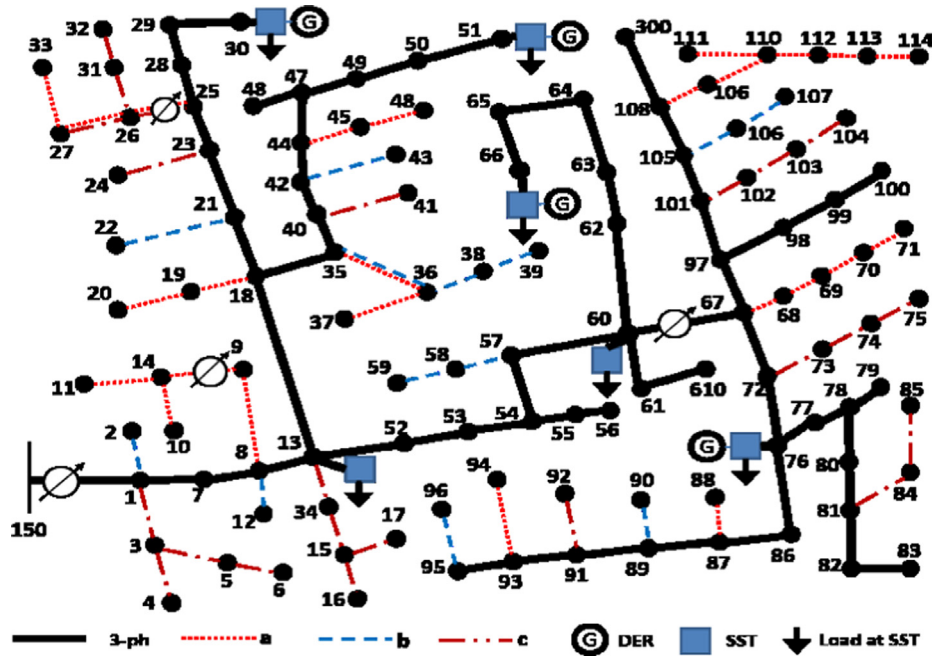


Fig. 2. Modified IEEE-123 test feeder with integrated DERs and SSTs.

primary side of the SST is only determined by SST var control in both UPF and var control modes, while the gateway active power is the net injection/consumption from DERs and loads as presented in (11) [33]. Recent research shows that the capacity rating of all three stages in the SST has increased to 270 kVA or at similar level. Moreover, multiple SSTs can be connected in parallel to serve many aggregated customers at the same node [34]. It is important for the DSOs and customers to size the loads and DERs according to the SST ratings during system design or restructuring.

$$Q_{load} = Q_{DAB} = Q_{SST} \quad (10)$$

$$|P_{DER} - P_{load}| \leq P_{SST} \quad (11)$$

The above features and constraints of the SST implementation will be discussed and modeled in Section 3.3.

### 3. Three-phase unbalanced OPF algorithm

This section describes the primal-dual interior point method (PDIPM) by fitting the constraints that have been mentioned in the previous section.

#### 3.1. Generalized OPF using PDIPM

The OPF formulation is shown in rectangular coordinate format in (13)–(18). The objective is to minimize a function  $F$ , which is the sum of generation costs  $f$ .

$$\text{Min } F(x) = \sum_x f(x) \quad (12)$$

Subject to

$$x = [x_1 \ x_2 \ x_3 \ x_4 \ x_5] = [P_g \ Q_g \ V_R \ V_M \ x_z]^T \quad (13)$$

$$f(x) = [f_{poly}(x) f_z(x)]^T \quad (14)$$

$$G(x) = 0 \quad (15)$$

$$H(x) \leq 0 \quad (16)$$

$$x_{min} \leq x \leq x_{max} \quad (17)$$

where  $x$  is a vector of independent variables;  $V_R$  and  $V_M$  are real and

imaginary parts of nodal voltage, respectively;  $P_g$  and  $Q_g$  are active and reactive power injections from controllable DERs and other devices;  $x_z$  is customer defined variables;  $f_{poly}(x)$  is classic quadratic generation cost;  $f_z(x)$  is customer-defined cost function (e.g. piecewise);  $G(x)$  and  $H(x)$  are equality and inequality system constraints, respectively;  $x_{max}$  and  $x_{min}$  are linear upper and lower limits to variable  $x$ .

#### 3.1.1. General formula of cost function $f$

The first and second order partial derivatives of cost function fare given as:

$$\nabla f(x) = \frac{\partial f_{poly}}{\partial x} + \frac{\partial f_z}{\partial x}, \quad \nabla^2 f(x) = \frac{\partial^2 f_{poly}}{\partial x^2} + \frac{\partial^2 f_z}{\partial x^2} \quad (18)$$

$$f_{poly}(x) = a_0 + a_1 P_g + a_2 P_g^2 \quad (19)$$

$$\nabla f_{poly}(x) = a_1 P_g + 2a_2 P_g, \quad \nabla^2 f_{poly}(x) = 2a_2 \quad (20)$$

where  $a_0$ ,  $a_1$ , and  $a_2$  are the polynomial factors. The formulation of piecewise cost as a customized function,  $f_z$  is discussed in part B of this section.

#### 3.1.2. General formula of equality constraints $G(x)$

$$G(x) = [G^P G^Q G^V G^M \dots G^z]^T \leftrightarrow [\lambda^P \lambda^Q \lambda^V \lambda^M \dots \lambda^z]^T \quad (21)$$

The elements in equality constraint vector  $G(x)$ , shown in (21), is explained below where  $\lambda$  is the dual variable used as Lagrange multipliers.  $G^P$  and  $G^Q$  are nonlinear nodal active and reactive power balance constraints given as the mismatch between total branch injecting power ( $P_{inj}$ ,  $Q_{inj}$ ), and nodal specified power ( $P_g - P_D$ ) and ( $Q_g - Q_D$ ). The corresponding dual variables  $\lambda^P$  and  $\lambda^Q$  can be used to represent the nodal shadow prices of power supply which may be used to derive the control signals for economic operation [33].

$$G^P = P_{inj} - (P_g - P_D), \quad G^Q = Q_{inj} - (Q_g - Q_D) \quad (22)$$

where

$$P_{inj} = V_R I_R - V_M I_M, \quad Q_{inj} = V_M I_R + V_R I_M \quad (23)$$

$I_R$  and  $I_M$  can be found using decoupled rectangular admittance matrices of (5).  $P_g$  and  $Q_g$  are nodal power generation as represented by variables  $x_1$  and  $x_2$ . The var injection at SST ( $Q_{SST}$ ) is also considered as a

reactive power source.  $P_D$  and  $Q_D$  are equivalent demand from ZIP load in (9). The nodal voltage magnitude limit can be dealt with nonlinear constraints in the rectangular coordinates. The equality voltage limit is only applicable for PV nodes (if there are any) which have the same upper and lower limits, such as  $=V_{max} = V_{min}$ .

$$G^V = V_R^2 + V_M^2 - V_{max}^2 \quad (24)$$

$G^Z$  is the optional customized nonlinear equality constraint defined by the user as needed. Any variable including customized variable  $x_z$ , with the same upper and lower limits, are included in the linear equality constraint  $G^z$  as presented in (25).  $A_{EQ}$  is the incidence matrix and  $B_{EQ}$  equals the variable equality limit.

$$G^z = A_{EQ} \cdot x_z - B_{EQ} \quad (25)$$

The first and second order partial derivatives of  $G(x)$  are given in general format as:

$$\nabla_{G(x)} = \left[ \frac{\partial G^P}{\partial x} \frac{\partial G^Q}{\partial x} \frac{\partial G^V}{\partial x} \frac{\partial G^M}{\partial x} \frac{\partial G^z}{\partial x} \right]^T \quad (26)$$

$$\nabla_{G(x)}^2 = \frac{\partial^2(G^P\lambda^P)}{\partial x^2} + \frac{\partial^2(G^Q\lambda^Q)}{\partial x^2} + \frac{\partial^2(G^V\lambda^V)}{\partial x^2} + \frac{\partial^2(G^M\lambda^M)}{\partial x^2} + \frac{\partial^2(G^z\lambda^z)}{\partial x^2} \quad (27)$$

### 3.1.3. General formula of inequality constraints $H(x)$

The elements in the inequality constraint vector  $H(x)$  are explained below:

$$H(x) = [H^f \ H^t \ H^{V+} \ H^{V-} \dots H^z]^T \leftrightarrow [\mu^f \ \mu^t \ \mu^{V+} \ \mu^{V-} \dots \mu^z]^T \quad (28)$$

The Lagrange multipliers  $\mu$  are the dual variables.  $H^f$  and  $H^t$  are nonlinear constraints on branch flows at the “from” and “to” ends in terms of squared power, shown in (29), or squared current, shown in (30), depending on the system security requirements:

$$H^f = (S^f)^2 - (S_{max}^f)^2, \ H^t = (S^t)^2 - (S_{max}^t)^2 \quad (29)$$

Or

$$H^f = (I_R^f)^2 + (I_M^f)^2 - (I_{max}^f)^2, \ H^t = (I_R^t)^2 + (I_M^t)^2 - (I_{max}^t)^2 \quad (30)$$

$$S^f = (V_R^f I_R^f + V_M^f I_M^f) + j(V_M^f I_R^f - V_R^f I_M^f) \quad (31)$$

where  $I_R^f, I_M^f, I_R^t,$  and  $I_M^t$  can be found using (6), (7), and (8).  $V_R^f, V_M^f, V_R^t,$  and  $V_M^t$  are the real and imaginary parts of voltages at “from” and “to” ends of branches. The “to” end branch flow  $S^t$  can be found in a similar way. The inequality voltage limits are evaluated only for PQ nodes ( $V_{min} < V < V_{max}$ ) as nonlinear constraints in (32).

$$H^{V+} = V_R^2 + V_M^2 - V_{max}^2, \ H^{V-} = -(V_R^2 + V_M^2) + V_{min}^2 \quad (32)$$

$H^z$  is optional customized nonlinear inequality constraint defined by user as needed. Such an example is presented in part C of this section for SST implementation. The first and second order partial derivatives of  $H(x)$  are:

$$\nabla_{H(x)} = \left[ \frac{\partial H^f}{\partial x} \frac{\partial H^t}{\partial x} \frac{\partial H^{V+}}{\partial x} \frac{\partial H^{V-}}{\partial x} \frac{\partial H^z}{\partial x} \right]^T \quad (33)$$

$$\nabla_{H(x)}^2 = \frac{\partial^2(H^f\mu^f)}{\partial x^2} + \frac{\partial^2(H^t\mu^t)}{\partial x^2} + \frac{\partial^2(H^{V+}\mu^{V+})}{\partial x^2} + \frac{\partial^2(H^{V-}\mu^{V-})}{\partial x^2} + \frac{\partial^2(H^z\mu^z)}{\partial x^2} \quad (34)$$

### 3.1.4. Build Lagrange function

$$L(x, \lambda, \mu, s) = F(x) + \lambda^T G(x) + \mu^T (H(x) + s) - \sigma \sum \ln(s) \quad (35)$$

There are four variables in the Lagrange function, presented in (35):  $x$  is the vector of primal independent variable;  $\lambda$  and  $\mu$  are vectors of Lagrange multipliers (dual variables) assigned to equality and inequality

constraints;  $s$  is a vector of the slack variable; and  $\sigma$  is the barrier factor. Taking partial derivatives of the Lagrange function with respect to each variable yields:

$$\nabla_{L(x,\lambda,\mu,s)} = [L_x \ L_y \ L_\mu \ L_s]^T \quad (36)$$

The KKT optimality conditions for the OPF problem are satisfied when the first order Lagrange derivatives of (36) are all equal to zero, the barrier constant  $\sigma$  tends to zero, and the inequality dual variable  $\mu$  is nonnegative [35]. They are defined as:

$$R_1 = L_x \rightarrow 0, \ R_2 = \max\{L_\lambda^G, L_\lambda^H\} \rightarrow 0, \quad (37)$$

$$R_3 = \mu^T s \rightarrow 0, \ R_4 = F^{j+1}(x) - F(x) \rightarrow 0. \quad (38)$$

where  $j$  denotes the iteration number;  $R_1$  represents the stationary condition that confirms the unique optimum  $x^*$  in the defined problem. All equality and inequality constraints are satisfied by  $R_2$ , which is the feasibility condition;  $R_3$  depicts the complementary condition which assures that the barrier parameter tends to zero;  $R_4$  ensures that the objective function value reaches an equilibrium. To reach the optimal point of KKT conditions, the second order derivative (Hessian matrix) of the Lagrange function is utilized, as presented below:

$$\nabla_{L(x,\lambda,\mu,s)}^2 = \begin{bmatrix} L_{xx} & \dots & L_{xs} \\ \vdots & \ddots & \vdots \\ L_{sx} & \dots & L_{ss} \end{bmatrix} \quad (39)$$

Let  $W = [x, \lambda, \mu, s]^T$ , variables  $x, \lambda, \mu,$  and  $s$  are updated using the Newton–Raphson iterative method in (40) and (41).

$$\nabla_W = (\nabla_L^2)^{-1} (-\nabla_L) \quad (40)$$

$$W^{j+1} = W^j + \nabla_W \quad (41)$$

### 3.2. Modifications from user-defined cost functions

Piecewise generation costs are included as an example of customer defined objective function in this paper. The customized cost function is defined based on (14) as:

$$f_z(x) = f_{pw}(x) = price_i(P_g - P_D) + C_{pw_i} \quad (42)$$

where  $i \in \mathbb{Z}$  refers to the sequence of price segments and  $P_{i-1} \leq P_g \leq P_i; C_{pw_i}$  is the cumulative cost for each segment. Since the partial derivatives of  $f_{pw}$  can only be evaluated in discontinuous segments, a new customized constrained variable  $x_{pw}$  is created equal to  $f_{pw}$ :

$$x_z = x_{pw} = f_{pw}(x) \quad (43)$$

This new variable  $x_z$  is added to the independent variable vector  $x$  as shown in (13). The dimension of  $x_{pw}$  is equal to the total number of generations in three phase with piecewise cost functions. The first and second order derivatives of  $f_{pw}$  are given below:

$$\nabla f_{pw}(x) = \frac{\partial f_{pw}}{\partial x} = \frac{\partial f_{pw}}{\partial x_{pw}} = 1 \quad (44)$$

$$\nabla^2 f_{pw}(x) = 0 \quad (45)$$

The linear constraints for  $x_{pw}$  associated with  $P_g$  will be included in  $H^z$  as in (28), and can be expressed as a linear matrix format:

$$\begin{bmatrix} price_i - 1 \\ x_{pw} \end{bmatrix} \leq \begin{bmatrix} P_g \\ price_i P_i - C_{pw_i} \end{bmatrix} \quad (46)$$

### 3.3. Modifications from SST implementation

The SST implementation may change the OPF model by modifying variables and constraints due to the exclusive features introduced earlier in Section 2.2. Table 2 provides a list of SST control modes and their

**Table 2**  
Modifications for SST control modes.

Mode	Modifications to OPF formulation	
1	$Q_D = 0$	1. Enforce linear variable constraint $P_g$ by SST rating.
2	$\frac{\partial S_{ZIP}}{\partial V} = 0$	1. Enforce linear variable constraint $P_g$ by SST rating. 2. Add new variable $Q_{SST}$ to $x_2$ with new nonlinear inequality constraint.

implementation. SST control mode 1 is unity power factor (UPF) which signifies zero reactive injection/consumption at the coupling point. In control mode 2, the SST can regulate the var injection/consumption based on external control signal sent by the DSO. In general, SSTs will set node type to PQ node. In case 1, the reactive injection or consumption from DERs and loads are filtered out to be zero by the DAB and inverter. In addition, the nonlinearity of ZIP loads will be removed since the customer terminal voltage is always regulated to 1.0 p.u. These changes in case 1 are also applicable to the other cases. In mode 1, if DER is installed, the DER active power limit is restricted by SST capacity rating as below:

$$\max(-S_{SST}, P_g^{min}) \leq P_g \leq \min(S_{SST}, P_g^{max}) \quad (47)$$

In mode 2, new variable  $Q_{SST}$  is added to variable  $x_2$  as controllable reactive generation, represented in (48). The  $Q_{SST}$  limit must address the coupling with DER active power generation and load consumption in a new customized non-linear equality constraint to satisfy the SST rating as shown in (49).

$$-\sqrt{S_{SST}^2 - (P_g - P_D)^2} \leq Q_{SST} \leq \sqrt{S_{SST}^2 - (P_g - P_D)^2} \quad (48)$$

$$H^z = (P_g - P_D)^2 + Q_{SST}^2 - S_{SST}^2 \quad (49)$$

## 4. Test results

### 4.1. Modified IEEE-123 test feeder

The IEEE-123 test feeder is known as a standard unbalanced test system [36]. The original system has been modified by installing PV based DERs at nodes 66, 51, 76, and 30, and SSTs at nodes 66, 51, 76, 30, 13, and 60. Fig. 2 shows the diagram of the modified IEEE-123 system. The capacity and generation cost of DERs and transmission supply are listed in Table 3 and Table 4, respectively. DER production cost function and transmission supply costs are modeled as the commonly used piecewise linear and quadratic polynomial functions, respectively. From the feeder specifications, it is found that the original loads are highly unbalanced, as loads on phases A and C are approximately 36% and 21% higher respectively than the load on phase B. Therefore, each DER has a different capacity and cost segments on each phase. Consequently, the SSTs are also installed with different capacity ratings on each phase, as shown in Table 5. The nodal voltage magnitude constraint is set between 0.95 and 1.05 p.u. The voltage regulator at substation 150 has reduced 5 taps on each phase, and the other regulators at 9–14, 25–26, 60–67 have zero tap setting in this test. For the performance evaluation, three cases are studied: No SST, SST mode 1, and SST mode 2. The results are compared and discussed in the next subsection.

**Table 3**  
Generation costs of Transmission supply.

Node	$P_{max}$	$P_{min}$	$a_0$	$a_1$	$a_2$
150	2000	-2000	140	25.5	.24

**Table 4**  
Generation costs of DER in modified IEEE 123 test feeder.

Node	Phase	$P_{max}$	$P_1$	$P_{r1}$	$P_2$	$P_{r2}$	$P_3$	$P_{r3}$
66	A	522	296	15	470	20	522	32
	B	360	204	15	324	20	360	32
	C	432	245	15	389	20	432	32
51	A	487	261	13	435	21	487	23
	B	336	180	13	300	21	336	23
	C	403	216	13	360	21	403	23
76	A	470	244	16	383	24	470	27
	B	324	168	16	264	24	324	27
	C	389	202	16	317	24	389	27
30	A	360	90	20	252	23	360	28
	B	240	60	20	168	23	240	28
	C	288	72	20	202	23	288	28

**Table 5**  
SST location and rating.

Node	$S_{SST, A}$ (kVA)	$S_{SST, B}$ (kVA)	$S_{SST, C}$ (kVA)
66	600	400	480
51	540	360	430
76	520	350	420
30	400	260	300
13	300	200	240
60	300	200	240

### 4.2. Results of test cases

The proposed OPF is performed on a computer with Intel core i7 2.20 GHz processor and 16 GB RAM. The convergence test of the OPF is recorded during the maximum penetration occurrence. Convergence test result is provided in Fig. 3 with all the KKT conditions mentioned earlier ( $R_1$  to  $R_4$ ). Tolerance level is set to  $10^{-6}$  for each of the conditions. It takes 30, 32, and 30 iterations for the No SST, SST mode 1 and SST mode 2 cases, respectively to converge. Computation times for the three cases are 3.943, 3.624, and 3.249 s, respectively.

Fig. 4 depicts the impact of maximum and no DER penetration events for phase A on energy prices during peak loading condition for all three cases. The maximum DER injection reverses the active power flow at the substation node. It is observed from the economic dispatch results that the total generation from DERs is higher than the total demand for maximum penetration which results in negative power flow at the substation node as depicted in Fig. 4(a). Since the optimal solutions of OPF are within the security constraints and the implementation of SSTs does not affect the constrained conditions, the generation dispatch of DERs in all three cases is identical. However, in SST modes 1 and 2, due to the control architecture presented in Table 2, the voltage profile at the SST nodes are being controlled. Since voltage sensitive ZIP loads are considered and voltage is being bounded in the lower band, the total active power available at the substation increases for selling back to the bulk energy market due to the decrease in demand. DERs at node 30, 76, 51, and 76 are located 3700, 3850, 4100, and 4550 feet away from the substation, respectively. The DSO aggregates the cheaper energy from DERs and sells it in the wholesale market. The shadow prices appear generally lower near the DER nodes and higher near the substation due to reversal of the power flow. The alternative events are also presented in Fig. 4(b) when there is no DER penetration. For different cases of SST, power supplied from the substation will vary. In both the SST modes, the power delivered from the substation is lower than when using conventional transformer. These zero DER cases naturally show lower shadow prices near the substation and higher prices further along the feeder since the entire energy is being delivered from the substation. Scenarios for shadow price are

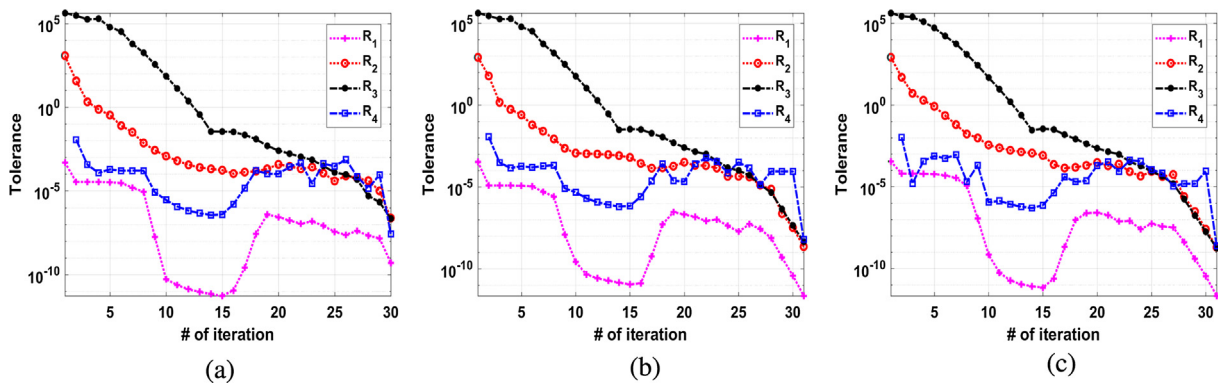


Fig. 3. Convergence test during max penetration (a). No SST; (b). SST mode 1; (c). SST mode 2.

presented in Fig. 4(c). Since implementation of SST can regulate the voltage level, and because voltage sensitive ZIP loads consume less energy when the voltage is lower, the demand varies between the no SST and the two SST modes. The SST modes can reduce the load consumption, as demonstrated in Fig. 4(d).

The total shadow price for one day is found by using the OPF by subtracting the total dollar amount of selling power to the bulk generation from the total amount purchased from the wholesale market. A QSTS simulation is conducted using the presented OPF methodology in 15 min intervals for an entire day. The total shadow price for marginal generation and voltage boundary is presented in Table 6 for all three phases in different SST modes. The table clearly shows that the voltage profile flattens out within the minimum and maximum voltage

boundaries, and the total shadow price also decreases when using the SST. Since SST mode 2 with reactive power capability provides more control over the voltage, it also minimizes the price more than in the SST mode 1.

Fig. 5 provides the QSTS analysis of voltage profile of Phase A. Comparing all three cases, it is clear that SST modes lead to flatter voltage profiles than the no SST mode. Since SST mode 2 has reactive power control capability, it is more effective in flattening the profile than with SST mode 1.

### 5. Conclusion

The increasing installation of DERs along with new investments on

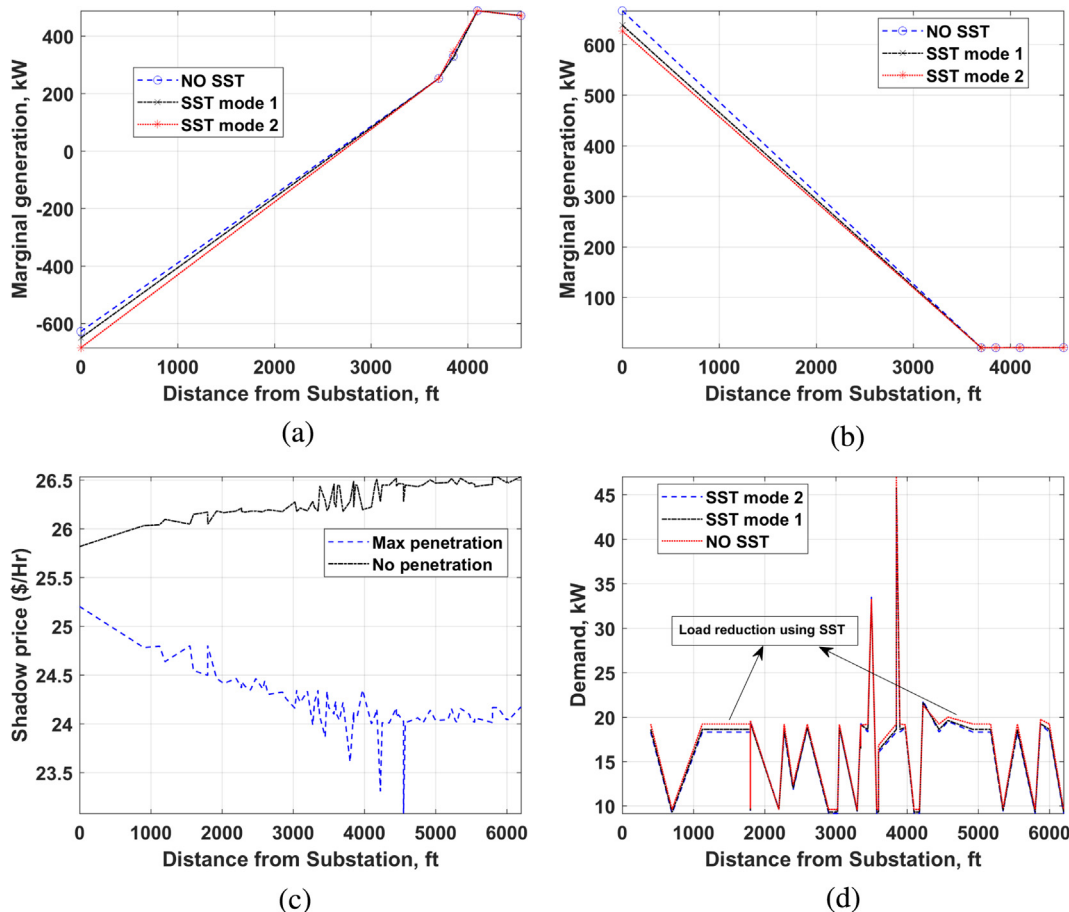


Fig. 4. (a). Generation during maximum DER penetration in Phase A; (b). Generation during no penetration in Phase A; (c). Price during maximum and no penetration in Phase A; (d). Demand using different SST modes in Phase A.

**Table 6**  
Voltage boundary and total shadow price for different SST modes.

Mode	No SST			SST Mode 1			SST Mode 2		
	A	B	C	A	B	C	A	B	C
$V_{max}(p.u)$	1.0438	1.0294	1.0387	1.0312	1.0183	1.0293	1.0283	1.0132	1.0279
$V_{min}(p.u)$	0.9839	0.9763	0.9945	0.9786	0.9827	0.9995	0.9790	0.9846	1.0007
Total Shadow Price(\$)	2664.49	2139.62	2383.57	2627.29	2112.83	2357.92	2597.41	2098.37	2334.73

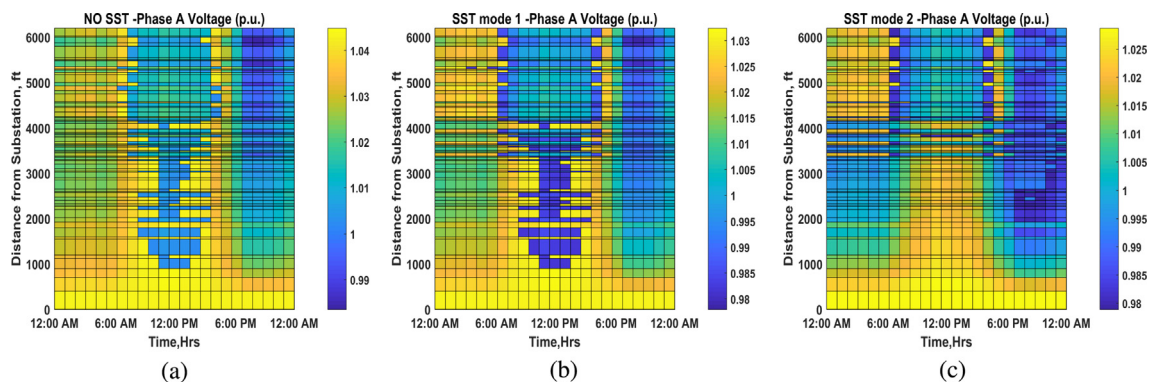


Fig. 5. Time-varying voltage profile (a) No SST; (b) SST mode 1; (c) SST mode 2.

infrastructure improvement packs the promise to enable the aging distribution system to evolve into a smart grid paradigm with increased controllability. A generalized three-phase unbalanced OPF algorithm is extended to perform optimization and control by an entity such as the DSO to aggregate the profitability of each resource while satisfying security constraints. The algorithm structure is general enough to adopt new user-defined device models and constraints. The feature of reactive var injection/absorption control by the SST is an important instrument to support DER penetration and renewable energy harvesting, especially in distribution networks featuring high R/X ratio conductors. Based on results obtained by the OPF method applied to an IEEE test feeder, the coordination between DER and SST in var control mode presents the most potential benefit of economic operation, voltage regulation, and system efficiency improvements. The proposed OPF algorithm also presents potential value in optimal design and restructuring of the distribution feeders. Extended research can be conducted using this OPF algorithm to control voltage regulators and capacitor banks for higher efficiency in system operations. Several other applications such as conservation voltage reduction, demand response, etc. may also be introduced.

**Acknowledgments**

Authors are grateful for the financial support received from the FREEDM Center for the first author during his doctoral studies at Missouri S&T.

**References**

[1] Office of Electric Transmission and Distribution, Grid 2030: A National Vision for Electricities Second 100 Years Jul 2007, U.S. Dept. of Energy. Available: <http://energy.gov/>.  
 [2] Hadjsad N, Sabonnadire J. Power systems and restructuring. London: Wiley; 2009.  
 [3] International Renewable Energy Agency, Renewable Energy Technologies: Cost Analysis Series, vol. 1, no. 4/5, June 2012.  
 [4] U.S. Dept. of Energy, 2010 Smart Grid System Report, Feb 2012. Available: <https://www.smartgrid.gov/>.  
 [5] Energy Regulatory Commission (CRE) in France. Available: <https://www.smartgrid.gov/>.  
 [6] Hambridge S, Huang AQ, Yu R. Solid State Transformer (SST) as an Energy Router: Economic Dispatch Based Energy Routing Strategy, in Proc. of IEEE Energy Conversion Congress and Exposition, Montreal, QC, 2015.

[7] Huang AQ. Medium-voltage solid-state transformer: technology for a smarter and resilient grid. IEEE Ind Electron Mag 2016;10(3):29–42.  
 [8] Ye Q, Mo R, Li H. Multiple resonances mitigation of paralleled in-verters in a solid-state transformer (SST) Enabled ac Microgrid, in IEEE Trans. on Smart Grid, vol. PP, no.99, pp. 1–1.  
 [9] She X, Huang AQ, Burgos R. Review of the solid state transformer technologies and its' application in power distribution system. IEEE J Emerg Select Top Power Electron 2013;1(3):186–98.  
 [10] Shah D, Crow M. Stability design criteria for distribution system with solid state transformers, in IEEE Trans. on Power Delivery, IEEE Trans. on Power Delivery, vol. 29, no. 6, pp. 2588–2595, Apr 2014.  
 [11] Qin H, Kimball JW. Solid state transformer architecture using ac-ac dual active bridge converter. IEEE Trans Ind Electron 2013;60(9):3720–30.  
 [12] Shah D, Crow ML. Online volt-var control for distribution systems with solid state transformers. IEEE Trans Power Delivery 2016;31(1):343–50.  
 [13] Zhao T, Wang G, Bhattacharya S, Huang AQ. Voltage and power balance control for a cascaded h-bridge converter based solid-state transformer. IEEE Trans Power Electron 2013;28(4):1523–32.  
 [14] Power Systems Engineering Research Center, The 21st Century Substation Design Final Project Report, PSERC Publication 10–15, Sep 2010. Available: <http://www.pserc.wisc.edu/>.  
 [15] Zhao T, Yang L, Wang J, Huang A. 270 kVA Solid State Transformer Based on 10 kV SIC Power Devices, in Proc. of IEEE Electric Ship Technologies Symposium, Arlington, VA, 2007.  
 [16] Farivar M, Clarke CR, Low SH, Chandy KM. Inverter Var Control for Distribution Systems with Renewables, in Proc. IEEE International Conference on Smart Grid Communications, Brussels, 2011.  
 [17] Farivar M, Neal R, Clarke C, Low S. Optimal inverter VAR control in distribution systems with high PV penetration, in proc IEEE Power and Energy Soc. General Meeting, San Diego, CA, 2012.  
 [18] Dall'Anese E, Dhople SV, Giannakis GB. Photovoltaic inverter controllers seeking ac optimal power flow solutions. IEEE Trans Power Syst 2016;31(4):2809–23.  
 [19] Shaloudegi K, Madinehi N, Hosseini SH, Abyaneh HA. A novel policy for locational marginal price calculation in distribution systems based on loss reduction allocation using game theory. IEEE Trans Power Syst 2012;27(2):811–20.  
 [20] Sotkiewicz PM, Vignolo JM. Nodal pricing for distribution networks: efficient pricing for efficiency enhancing DG. IEEE Trans Power Syst 2006;21(2):1013–4.  
 [21] Sotkiewicz PM, Vignolo JM. Towards a cost causation-based tariff for distribution networks with DG. IEEE Trans Power Syst 2007;22(3):1051–60.  
 [22] Singh RK, Goswami SK. Optimum allocation of distributed generations based on nodal pricing for profit, loss reduction, and voltage improvement including voltage rise issue. Int J Electr Power Energy Syst 2010;32(6):637–44.  
 [23] Nick M, Cherkaoui R, Paolone M. Optimal allocation of dispersed energy storage systems in active distribution networks for energy balance and grid support. IEEE Trans Power Syst 2014;29(5):2300–10.  
 [24] Meng F, Chowdhury B, Chamana M. Three-phase optimal power flow for market-based control and optimization of distributed generations, in IEEE Trans. on Smart Grid, vol. PP, no. 99, pp. 1–1.  
 [25] Forsgren A, Gill PE, Wright MH. Interior methods for nonlinear optimization. Soc Ind Appl Math Rev 2002;44(4):525–97.  
 [26] Araujo LR, Penido DRR, Carneiro Jr. S, Pereira JLR. A Three-phase optimal power-flow algorithm to mitigate voltage unbalance. IEEE Trans Power Delivery

- 2013;28(4).
- [27] de Araujo LR, Penido DRR, de F, Vieira A. A multiphase optimal power flow algorithm for unbalanced distribution systems. *J Electr Power Energy Syst* 2013;53:632–42.
- [28] Garcia P, Pereira J, Carneiro Jr. S, Costa V, Martins N. Three-phase power flow calculations using the current injection method. *IEEE Trans Power Syst* 2000;15(2):508–14.
- [29] Kersting WH. *Distribution system modeling and analysis*. New York: CRC; 2007.
- [30] Bokhari A, et al. Experimental determination of the ZIP coefficients for modern residential, commercial, and industrial loads. *IEEE Trans Power Delivery* 2014;29(3):1372–81.
- [31] Byrd R, Nocedal J, Waltz R, Wu Y. On the use of piecewise linear models in nonlinear programming. *Math Program* 2013;137(1–2):289–324.
- [32] U.S. Dept. of Energy, The potential benefits of distributed generation and rate-related issues that may impede their expansion, Feb. 2007 [online]. Available: <http://www.energy.gov>.
- [33] Meng F, Haughton D, Chowdhury B, Crow M, Heydt G. Distributed generation and storage optimal control with state estimation. *IEEE Trans Smart Grid* 2013;4(4).
- [34] Wang F, She X, Wang G, Huang A, Burgos R. Parallel Operation of Solid State Transformer, in *Proc. of IEEE Energy Conversion Congress and Exposition*, Raleigh, NC, 2012.
- [35] Forsgren A, Gill PE, Wright MH. Interior methods for nonlinear optimization. *Soc Ind Appl Math Rev* 2002;44(4):525–97.
- [36] IEEE, PES Distribution System Analysis Subcommittees Distribution Test Feeder Working Group. Available: <http://www.ewh.ieee.org/soc/pes/dsacom/testfeeders/index.html>.